Quantifying the sensitivity of aerosol optical properties to the parameterizations of physico-chemical processes during the 2010 Russian wildfires and heatwave

Laura Palacios-Peña[1], Philip Stier[2], Raquel Lorente-Plazas[3], and Pedro Jiménez-Guerrero[1,4]

[1]Physics of the Earth, Regional Campus of International Excellence "Campus Mare Nostrum", University of Murcia, Spain.
[2]Atmospheric, Oceanic and Planetary Physics, Department of Physics, University of Oxford, UK.
[3]Dept. of Meteorology, Meteored, Almendricos, Spain.
[4]Biomedical Research Institute of Murcia (IMIB-Arrixaca), Spain.

Correspondence: Pedro Jiménez-Guerrero (pedro.jimenezguerrero@um.es)

Abstract. The impact of aerosol-radiation and aerosol-clouds interactions on the radiative forcing is subject to large uncertainties. This is caused by the limited understanding of aerosol optical properties and the role of aerosols as cloud condensation/ice nuclei (CCN/IN). On the other hand, aerosol optical properties and vertical distribution are highly related and their uncertainties come from different processes. This work attempts to quantify the sensitivity of aerosol optical properties (i.e. aerosol

5   optical depth; AOD) and their vertical distribution (using the extinction coefficient, backscatter coefficient, and concentrations species profiles) to key processes. In order to achieve this objective sensitivity tests have been carried out, using the WRF-Chem regional fully coupled model by modifying the dry deposition, sub-grid convective transport, relative humidity and wet scavenging. The 2010 Russian heatwave/wildfire episode has been selected as case study.

Results indicate that AOD is sensitive to these key processes in the following order of importance: 1) modification of relative

10 humidity, causing AOD differences up to 0.6; 2) modification of vertical convection transport with AOD differences around -0.4; and 3) the dry deposition with AOD differences up to -0.35 and 0.3. Moreover, these AOD changes exhibit a non-linear response. Both, an increase and a decrease in the RH result in higher AOD values. On the other hand, both, the increase and offset of the sub-grid convective transport lead to a reduction in the AOD over the fire area. In addition, a similar non-linear response is found when reducing the dry deposition velocity; in particular, for the accumulation mode where the concentration

15 of several species increases (while a decrease might be expected). These non-linear responses are highly dependent on the equilibrium of the thermodynamics system sulphate-nitrate-SOA (secondary organic aerosol). In this sense, small changes in the concentration of one species can strongly affect others, finally affecting aerosol optical properties. Changes in this equilibrium could come from modifications in relative humidity, dry deposition or vertical convective transport. By itself, dry deposition also presents a high uncertainty influencing the AOD representation.

1 Introduction

Since the First Assessment Report of the Intergovernmental Panel on Climate Change (IPCC), a wide scientific consensus identifies atmospheric aerosols and clouds as one of the forcing agents with a larger uncertainty in the climate system (Charlson et al., 1992; Schimel et al., 1996; Penner et al., 2001; Randall et al., 2007; Forster et al., 2007; Boucher, 2015). Atmospheric aerosols modify the Earth's radiative budget through aerosol-radiation interactions (ARI) and aerosol-cloud interactions (ACI). ARI lead to a redistribution of radiative energy in the atmosphere through scattering and absorption. In addition, ACI modify cloud microphysical properties and precipitation regimes as well as cloud effects on radiation (Randall et al., 2007; Boucher et al., 2013).

ARI and ACI are strongly dependent on aerosol optical properties and the ability of aerosols to act as cloud condensation nuclei (CCN) or ice nuclei (IN), which are controlled by the spatio-temporal aerosol distribution, the aerosol size, composition and mixing state (Stier et al., 2005). Thus, to determine and constrain the uncertainty in aerosol optical properties is a key issue for a better assessment of the uncertainty in aerosol effects.

Numerical models are useful tools for understanding the different processes influencing the atmospheric system, as aerosol optical properties. The complexity of how aerosols are treated in models varies widely, since these models take into account processes as emission, transport, deposition, microphysics and chemistry (Kipling et al., 2016). Differences in complexity primarily arise from representations of aerosol size distribution and mixing states. The most complex and realistic models are those considering the inclusion of ARI and ACI since they allow a fully-coupled interaction of aerosols, meteorology, radiation and chemistry. One example of these numerical models is WRF-Chem (Grell et al., 2005), used in this work. Notwithstanding the complexity of aerosol treatment in these models, there are still high uncertainties in processes representing the aerosol optical properties.

As stated by previous works (e.g. Palacios-Peña et al. (2017, 2018, 2019)), uncertainties in aerosol optical properties may be influenced by a number of factors, namely emissions; aerosol mass concentration; particle size representation (Balzarini et al., 2015); vertical distribution and location with respect to other forcing agents as clouds (Kipling et al., 2016); dry deposition and CCN (Romakkaniemi et al., 2012; Lee et al., 2013; Forkel et al., 2015); relative humidity (RH; Yoon and Kim, 2006; Zhang et al., 2012; Altaratz et al., 2013; Weigum et al., 2016); and aerosol internal mixing rules (Curci et al., 2019; Zhang et al., 2012).

Precisely, aerosol vertical distribution is high influenced by aerosol optical properties (Palacios-Peña et al., 2018, 2019). Henceforth, Kipling et al. (2016) investigated the uncertainty in the vertical layering of aerosol particles to different parameters: convective transport, emissions injection and size; vertical advection, boundary-layer mixing, entrainment into convective plumes, condensation, coagulation, nucleation, aqueous chemistry, aging of insoluble particles, Aitken transition to accumulation mode, dry deposition, in-cloud and below-cloud scavenging and re-evaporation. The convective transport and the in-cloud scavenging were found to be very important when controlling the vertical profile of all-aerosol components by mass and those with the highest influence on aerosol optical depth (AOD) (Kipling et al., 2016).

The representation of CCN has been also identified as another second-order source of uncertainty in aerosol optical properties, such as AOD. An increase in downward solar radiation was found by Forkel et al. (2015) and Romakkaniemi et al. (2012) when ACI were taken into account. This latter contribution found a relationship between a reduction in the AOD and CCN because the inclusion of ACI in numerical models leads to a reduction in CCN by the condensation kinetics of water during cloud droplet formation. This induces a reduction of the cloud droplet number, the cloud liquid water and, finally, an increase in downward solar radiation. In addition to AOD, CCN conditioned the uncertainty in ACI, as well as cloud occurrence and cloud-related processes (updraught speeds, precipitation processes, etc.). Because of that, the high uncertainty existing when modelling CCN was evaluated by Lee et al. (2013), finding that dry deposition was the most important process for this uncertainty over more than twenty-eight model parameters selected by expert elicitation, including nucleation, aerosol ageing, pH of cloud drops, nucleation scavenging, dry deposition, modal with mode separation diameter, emissions and production of secondary organic aerosols (SOA). These results, which are partly because wet deposition was not fully varied, were found in one model framework (with its own structural uncertainties).

Another source of uncertainty is the aerosol variability at scales smaller than the model's grid box, which can hamper the representation of aerosol optical properties. This fact was brought to light in Weigum et al. (2016), where the aerosol water uptake through aerosol-gas equilibrium reactions was established as one of the most affected processes by this variability. The inherent non-linearities in these processes result in large changes in aerosol properties which are exaggerated by convective transport. The uncertainties in RH also contribute to those of aerosol optical properties due to their dependence in hygroscopic growth (Yoon and Kim, 2006; Zhang et al., 2012; Altaratz et al., 2013; Palacios-Peña et al., 2019). Bearing in mind the uncertainties described above, the aim of this work is to shed some light on the uncertainties when representing aerosol optical properties. In order to achieve this objective, this contribution quantifies the sensitivity of aerosol optical properties and their vertical distribution (which may condition aerosol radiative forcing) to several aerosol processes and parameters. The sensitivity tests were carried out using the WRF-Chem regional fully-coupled model by modifying dry deposition, sub-grid convective transport, relative humidity and wet scavenging.

2 Methodology

Sensitivity tests have been conducted to assess the impact of the most relevant processes for representing aerosol optical properties. For that, the WRF-Chem model (Grell et al., 2005) version 3.9.1.1 has been utilized. The 2010 Russian heatwave/wildfires episode has been selected as a case study because of the literature available referring to this episode (see section 2.1). To achieve this objective, aerosol dry deposition velocity, sub-grid convective transport, aerosol water uptake and wet scavenging were the processes scaled. The degree of impact of these processes is evaluated by analyzing the AOD, different vertical profiles for extinction (α) and backscatter coefficient (β), and the concentration profiles of different aerosol species. The AOD is defined as the vertical integral of extinction in the total atmospheric column.

2.1 The 2010 Russian wildfires and heatwave episode

The 2010 Russian wildfires and heatwave episode occurred approximately from 25 of July to 15 of August 2010 and lasted a total of 22 days. This was an anomalous heatwave, termed as "mega-heatwave" by Barriopedro et al. (2011), with monthly mean temperatures in the summer months 5–9 °C higher than those for 2002–2009 due to a prolonged blocking anticyclone situation which triggered large wildfires (Bondur, 2011). This prolonged blocking situation has been attributed to the global warming leading to very high sea surface temperatures in several places around the world, due to the action of the ENSO (El Niño Southern Oscillation) which altered the atmospheric circulation by forcing quasi-stationary Rossby waves (Sedlàček et al., 2011; Lau and Kim, 2012; Trenberth and Fasullo, 2012). In addition, according to Rahmstorf and Coumou (2011) the 2010 July heat record in Moscow was caused by the climate warming with approximate 80 % probability.

With respect to air quality, this is a well-known and widely studied episode. Many of these works analyzed the physico-chemical characteristics of the smoke from wildfires and the effects on air quality of the transport (both particles and trace gases) to surrounding areas (Zvyagintsev et al., 2011; Witte et al., 2011; van Donkelaar et al., 2011; Gorchakov et al., 2014; Safronov et al., 2015); medium-range transport (e.g. Finland) (Portin et al., 2012; Mielonen et al., 2013) or long-range transport, even reaching Greece (Diapouli et al., 2014).

Among all these reasons, this heatwave has been extensively investigated because of the particularly significant interactions between meteorology and chemistry/particles during this strong air pollution episode (Makar et al., 2015b, a; Kong et al., 2015). This episode was one of the case studies within the COST Action ES1004 EuMetChem (European framework for online integrated air quality and meteorology modelling; see http://www.eumetchem.info/) chosen from the previous experience of Phase 2 of the Air Quality Modelling Evaluation International Initiative (AQMEII; Galmarini et al., 2015).

The effects of air pollution on meteorology where evinced by Konovalov et al. (2011), Chubarova et al. (2012) and Wong et al. (2012) among others. These studies demonstrated changes in atmospheric regional conditions caused by a modification in the composition of atmospheric gases; and also because of changes in optical and radiative characteristics of aerosols coming from the fire emissions. Gorchakov et al. (2014) detected a regional mean AOD of 1.02 ± 0.02 and a very high single-scattering albedo (0.95); and estimated a regional mean aerosol radiative forcing at the top and the bottom of the atmosphere of -61 ± 1 and -107 ± 2 W m^{-2}, respectively.

When aerosol interactions were taken into account, a reduction of solar radiation on the ground up to 50 W m^{-2} in diurnal averages and in the near-surface air temperature between 0.2 and 2.6 °K was evaluated on a regional scale over most of eastern Europe. Similarly, a reduction in the planetary boundary layer (PBL) height from 13 to 65 % and the vertical wind speed from 5 to 80 % were found by Péré et al. (2014). Baró et al. (2017) reported similar results on surface winds caused by a decrease of the shortwave downwelling radiation at the surface, leading to a reduction of the 2-m temperature and hence reducing the turbulent flux and developing a more stable PBL. This cooling increases both the surface pressure over the Russian area and the (with values around +3.5 %). In the same case, Forkel et al. (2016) manifested a reduction between 10 and 100 W m^2 in the average downward short-wave radiation at the ground level and a drop in the mean 2-m temperature of almost 1 °K over the area where the fires took place. On the other hand, Péré et al. (2015) evaluated the impact of aerosol solar extinction on the

photochemistry, resulting in a reduction of the photolysis rates of NO_2 and O_3 up to 50 % (daytime average) due to the aerosol
extinction along the aerosol plume transported, as well as a reduction of the formation of secondary aerosols.

2.2 Model setup

As aforementioned, the version 3.9.1.1 of the fully coupled on-line WRF-Chem model (Grell et al., 2005) was used in order to
simulate transport, mixing, and chemical transformation of trace gases and aerosols coupled to the meteorology (thus including
ARI and ACI processes, among others).

Figure 1 displays the target domain of the simulations which covered Europe with a horizontal resolution of ~ 23 km.
However, in order to focus on the aerosol effects, a smaller window covering between 40 and 65 ° N and 20 and 60 ° E (green
box in Figure 1) was defined.

The definition of the modelling domain, initial and boundary meteorological and chemical conditions and different emissions
has been built on the previous experiences of the COST Action EuMetChem and Phase 2 of the AQMEII initiative. However, in
this case the simulations are continuous runs instead of reinitialized every 48 hours (two-day time slices) as done in AQMEII
and EuMetChem methodologies (Forkel et al., 2015). A spin-up period of five days has been considered for running the
sensitivity tests.

Meteorological initial and boundary conditions (3-hourly data and 0.25° resolution) were provided by the European Cen-
tre for Medium-Range Weather Forecasts (ECMWF) operational archive. Chemistry boundary conditions (3-hourly data and
1.125° resolution) for the main trace gases and particulate matter concentrations were taken from the ECMWF Integrated
Forecasting System – Model for Ozone and Related Chemical Tracers (IFS-MOZART) model run in the (MACC-II) project
(Monitoring Atmospheric Composition and Climate-Interim Implementation; Inness et al., 2013).

Annual anthropogenic emission (~ 7 km resolution), whose details are described in Im et al. (2015a, b), came from the
Netherlands Organization for Applied Scientific Research (TNO) MACC emissions inventory (http://www.gmes-atmosphere.
eu/; Pouliot et al., 2012; Kuenen et al., 2014; Pouliot et al., 2015). CH_4, CO, NH_3, total Non-Methane Volatile Organic Com-
pounds (NMVOCs), NO_x, PM (PM_10 and $PM_{2.5}$) and SO_2 were available by 10 activity sectors. Schaap et al. (2005) provided
temporal profiles (diurnal, day-of-week, seasonal) and vertical. Biomass burning emission data of the total PM emissions (spa-
tial resolution of 0.1 °) were derived from the project IS4FIRES (Integrated monitoring and modelling system for wild-land
fires; Sofiev et al., 2009). Other biomass burning emission species were estimated after Im et al. (2015b). No heat release due
to the fires was considered. Table 1 summarizes the physico-chemical parameterizations and schemes used in the simulations.

The skills of the model to represent AOD during this episode have been evaluated in depth in Palacios-Peña et al. (2018) and
Palacios-Peña et al. (2019). The model skillfully represents low and mean AOD values albeit underestimates the high AOD
over the Russian area due to two different hypothesis: 1) not considering the fire emissions from small fires (Toll et al., 2015;
Wooster et al., 2005) or 2) a misrepresentation of the aerosol vertical profile based on the understated injection height of the
total biomass burning emissions found by Soares et al. (2015).

Atmospheric
Chemistry
and Physics
Discussions

2.3 Sensitivity tests

Table 2 summarizes the sensitivity tests carried out. As previously mentioned, the processes selected to be scaled include RH, dry deposition, sub-grid convective transport and wet scavenging. They were chosen because they are considered as key sources of uncertainty when modelling atmospheric aerosol properties and thus they are expected to impact the estimation of aerosol

155 optical properties (e.g. Ackermann et al. (1998); Lee et al. (2013); Quan et al. (2016), among many others).

RH highly impacts aerosol properties by affecting several processes as nucleation, chemistry or uptake of water through aerosol-gas equilibrium reactions (Ackermann et al., 1998). Because of that, our sensitivity test for this variable modified the RH in the aerosol module of WRF-Chem (precisely, in the part of the code when RH enters the aerosol module). Henceforth, RH modification only affects aerosol properties and not meteorology. Following the evaluation of this meteorological variable

160 conducted by Tuccella et al. (2012) and Žabkar et al. (2015), it was scaled to 0.9 (a reduction of 10 %). Although the translation into saturation only applies at saturation conditions, supersaturation values higher than 1 % are unlikely. Because of that, this variable could not be scaled by +10% (to 1.1), and hence the chosen upper values were 1.005 and 1.01; that is, 0.5 % and 1 % supersaturation respectively.

In this work, dry deposition velocity (DDV) is estimated by the MADE module (Ackermann et al., 1998) as in the Regional

165 Particulate Model (RPM; Binkowski and Shankar, 1995). But in contrast to RPM, MADE calculates and applies deposition velocities separately for each mode (Aitken, accumulation and coarse). The method uses the aerodynamic resistance, the settling velocity and Brownian diffusivity; and then, the Slinn and Slinn (1980)'s and Pleim et al. (1984)'s expressions are calculated by averaging the quantities over the kth moment of the distribution as in Kramm et al. (1992). The modification for our sensitivity test regarding dry deposition consists on scaled DDV by the values indicated in Table 2. Following Lee

170 et al. (2013), DDV has been scaled to 0.5 and 2 for the Aitken mode and 0.1 and 10 for the Accumulation mode. WRF-Chem configuration gives the opportunity to turn on/off the dry deposition of gases and aerosols. Thus, another sensitivity case corresponds to the WRF-Chem configuration with the dry deposition of aerosol turned off (aer_drydep_opt = 0 in the namelist of the model).

Analogously to dry deposition, sub-grid convective transport in WRF-Chem can be turned on/off. This process is parametrized

175 by a simple scheme (Grell and Dévényi, 2002) based on a convective parametrization developed by Grell (1993) and Grell et al. (1994). This scheme estimates the output temporal tendency (s^{-1}) separately in the bottom layer and the rest of the layers. Afterwards this tendency is applied to the chemical concentration for each species in order to estimate the sub-grid convective transport. This tendency has been modified in our sensitivity test as indicated in Table 2. Following the evaluations carried out by Doherty et al. (2005) and Quan et al. (2016), the output temporal tendency has been scaled to ± 50 %. Moreover, a case

180 with sub-grid convective transport turned off (chem_conv_tr = 0 in the model's namelist) has been run.

Aerosol wet scavenging in WRF-Chem follows the approach of Easter et al. (2004). This process is produced by impacting/interception and precipitation, when all aerosol species are assumed to be immediately wet-deposited. The model distinguishes between wet scavenging for large-scale and sub-grid stratiform and sub-grid convective clouds. Both, stratiform (wetscav_onoff) and convective (conv_tr_wetscav) wet scavenging can be turned on/off in WRF-Chem. A case in which

185 stratiform wet scavenging is turned off was run. This modification has been chosen because the evaluated episode was an anticyclonic situation without important convective clouds.

3   Results and discussion

In this section the results of the sensitivity of AOD representation to changes in RH, DDV, wet scavenging and convective transport are assessed, focusing on the Russian region affected by the heatwave-wildfire episode. Afterwards, a local evaluation
190 of the vertical profiles is carried out in order to establish the influence of each process on aerosol vertical profiles.

3.1   Changes in total AOD

Figure 2,top displays the modelled AOD at 550 nm for the base case. The rest of the Figure 2 depicts the differences between the sensitivity experiments and the base case. The top-right figure shows the mean bias. For the base case, high AOD values (up 0.5) are found over a large area of central Russia, including populated cities such as Moscow, Nizhny Novgorod or Kazan.
195 AOD values around 0.3, are found over a wider area close to the Finnish border (northwest of the domain) and over most of Belarus, Ukraine and the Black Sea (south of the domain). The lowest values (around 0.1) are found over central Europe. The changes of AOD in the sensitivity experiments are shown in the other pannels of Figure 2

Figure 2,*a*, *b* and *c* represent the sensitivity to RH: a decrease of 10% (L10RH); an increase of 0.5% (H05RH); and an increase of 1% (H1RH), respectively. As expected, a 10% decrease of the RH leads to a stronger response compared with the
200 experiments when RH increases since the percentage of modification is lower in the latter sensitivity tests. L10RH (Figure 2,*a*) experiment shows positive differences at the west of the Volga river, reaching values around +0.6. Oppositely, there are negative differences of -0.15 in the area placed eastern to the Volga. Meanwhile, the H05RH (Figure 2,*b*) experiment shows this positive (west)/negative (east) dipole over the fire-affected area but differences are lower than 0.15.The H1RH experiment (Figure 2,*c*) promotes an increase of AOD encompassing most of the fire-affected area with values around +0.2.

205 Figure 2,*d* stands for the No-Dry Deposition case (NO_DD): Figure 2,*e* and *f* are the experiments with Low and High Dry Deposition for the Aitken mode, respectively (LDDV_AIT and HDDV_AIT); and Figure 2,*g* and *h* represent the tests modifying the Accumulation mode (LDDV_ACC and HDDV_ACC). All the experiments related to changes in dry deposition (Figure 2,*d-h*) showed the strongest response located over the wildfires area, but less significant. Figures 2,*d*, NO_DD, and *e*, LDDV_AIT, have a similar spatial pattern of differences with positive changes (up to +0.35 and +0.2, respectively) at the
210 western Volga river. However, increasing the dry deposition in Aitken mode (Figure 2,*f*) and both increasing and decreasing the deposition in accumulation mode (Figures 2,*g* and *h*) provokes negative changes of AOD over the eastern Volga (around -0.3 in all of these cases).

Figure 2,*i* shows the No sub-grid Convective Transport (NO_CONV_TR) case and Figure 2,*j* the High sub-grid Convective Transport (HCONV_TR) case. Both of them evidence negative differences (up to -0.39 and -0.43, respectively) over the fire-
215 affected and downwind areas. However, the NO_CONV_TR case displays stronger positive differences over the northeastern part of the domain (up to +0.25) which do not occur for the HCONV_TR experiment. Figure 2,*k* indicates that the Low sub-grid

Convective Transport case (LCONV_TR) presents smooth differences. A dipole of positive and negative differences (which means higher and lower AOD than the base case) is found over all the domain, a bit stronger over the fire-affected area.

Finally, turning off the scavenging (Figure 2,*l*; NO_WS experiment) leads to positive differences over a large part of the area
220 with values higher than +0.2 over the north and west zones of the target domain.

3.2 Optical properties and concentration profiles of different species: disentangling the causes of AOD changes

In order to disentangle the cause of the differences in the sensitivity tests, this section discusses the vertical profiles of optical properties and concentration of several chemical species over specific locations of the target area. Figure 2, top-left displays where the spot where the vertical profiles are estimated. The choice of these locations claims to bring light to the behaviour
225 aloft over different places in the target area. Because of that, the locations where the time mean of AOD was minimum and maximum, respectively, were selected and named as Min-AOD and Max-AOD. A profile over Moscow, one of the most fire-affected cities, was also chosen to evaluate the fire plume effect downwind.

In addition to α, β and lidar ratio (LR), concentrations for different species were evaluated: elemental carbon (EC), primary organic aerosol (POA), secondary organic aerosol (SOA), sea salt (SEA), nitrate (NO_3^-), ammonia (NH_4^-) and sulphate (SO_4^{2-}).
230 Vertical profiles over the Max-AOD location are shown in Figure 3. α and β present similar profiles. The base case shows a profile with high values (above $0.6\,\mathrm{km}^{-1}$ for α and below $0.02\,\mathrm{km}^{-1}\mathrm{sr}^{-1}$ for β) at the surface. Both values decrease with height until around $0.2\,\mathrm{km}^{-1}$ for α and $0.005\,\mathrm{km}^{-1}\mathrm{sr}^{-1}$ at 900 hPa. Afterwards, values increase again to $0.3\,\mathrm{km}^{-1}$ for α and $0.01\,\mathrm{km}^{-1}\mathrm{sr}^{-1}$ at around $800\,\mathrm{hPa}$ (indicating the presence of aerosols associated to fire emissions aloft), where hereinafter decrease. Values are close to 0 above 600 hPa.

235 LR represents the ratio of the extinction and the backscatter coefficients and is usually used to characterize the type of particles. This variable ranges from 1 to $100\,\mathrm{sr}{-}1$ (Fernald et al., 1972). Following this definition, low LR values are expected for large and scattering particles and high LRs are expected for absorbing particles. Typical LRs at 532 nm are $20\text{-}35\,\mathrm{sr}{-}1$ for sea salt, $40\text{-}70\,\mathrm{sr}{-}1$ for desert dust, $70\text{-}100\,\mathrm{sr}{-}1$ for biomass burning aerosols and $45\text{-}75\,\mathrm{sr}{-}1$ for urban/continental aerosols (Müller et al., 2007). The vertical profile of LR displays low values of around $35\,\mathrm{sr}^{-1}$ at low heights. LR increases to values
240 between 50 and $60\,\mathrm{sr}^{-1}$ around 700 hPa. Higher up, between 500 and $300\,\mathrm{hPa}$, LR reaches values around $65\,\mathrm{sr}^{-1}$ which again, above $300\,\mathrm{hPa}$, decrease to $35\,\mathrm{sr}^{-1}$. A remarkable issue is that LR values are rather constant at levels close to the surface, contradicting the LR expected from observations. For example, Mielonen et al. (2013) measured the LR during the same forest-fire event in Finland. These authors found LR values of $60\text{-}70\,\mathrm{sr}^{-1}$ for layers below $2\,\mathrm{km}$, pointing to a mixture of biomass burning aerosols and other less absorbing aerosols. Conversely, in the upper layers the LRs were around $55\,\mathrm{sr}{-}1$,
245 which indicated the presence of polluted dust. This reveals the misrepresentation in the LRs by our simulations, which estimate LRs around $35\,\mathrm{sr}{-}1$ (typical LR values for sea salt particles) over areas with a high concentration of biomass burning aerosols (LR should typically reach values higher than $60\,\mathrm{sr}{-}1$).

In order to assess which species has the strongest influence on α and β, and also which chemical species presents the highest sensitivity in the designed experiments, profiles for the different species are shown in Figure 3, 5 and 7. Overall, total
250 concentration is highly determined by the dry concentration, as expected for a heatwave episode. In addition, Figure 4, 6 and 8

quantify the mean absolute error (MAE) of each experiment with respect to the base case, and in colors, the normalized MAE (NMAE). This latter statistical figure has been defined by normalizing the mean absolute error with respect to the values in the base case in order to show the magnitude of the relative changes in each sensitivity test for each variable evaluated.

3.2.1 Sensitivity to the relative humidity

255   When the sensitivity tests are evaluated over the MAX-AOD location, the experiments changing the RH present a singular response. When RH increases (H05RH and H1RH), the profile of optical properties also increases, as well as the AOD. MAE for the profiles (Figure 4) of α (β) are 0.0101 (0.0005) and 0.0159 (0.0004), for the case in which RH is scaled to 0.5 % (H05RH) and 1 % (H1RH) respectively, and NMAE are 0.4 (0.4) and 0.6 (0.5). These differences could be caused by the high dependence of AOD on water uptake, which finally depends on RH, as indicated by Ginoux et al. (2006); Yoon and

260   Kim (2006); Altaratz et al. (2013); Palacios-Peña et al. (2017, 2018, 2019). Thus, an increase in RH affects the hygroscopic growth, resulting in larger particles. For this reason, a reduction of optical properties is expected when RH decreases (L10RH experiment). However, the results indicate an increase in AOD and optical properties profiles (MAE 0.0162 and NMAE 0.6 for α; and 0.0005 and 0.7 for β). This response is the result of an increase of NO_3^- (MAE 0.8209 and NMAE 0.6) and, in particular, of SOA (MAE 0.2054 and NMAE 0.9).

265   The concentrations of inorganic species are controlled by the so-called sulphate-ammonium-nitrate-water equilibrium (Seinfeld and Pandis, 2006). NO_3^- and NH_4^- present a deliquescence RH of approximately 60 % (Saxena et al., 1986). However, SO_4^{2-} absorbs water at nearly all RH. As exposed by Weigum et al. (2016), due to the RH absorption by the SO_4^{2-}, the equilibrium is dominated by the reaction in which ammonia neutralizes sulphuric acid and drives the equilibrium towards the aerosol phase ((NH_4)$_2SO_4$). Therefore, ammonia can neutralize nitrate resulting in aerosol phase (NH_4NO_3) only when the

270   total amount of sulphate has been neutralized (i.e. in areas with high concentrations of ammonia and/or low concentrations of sulphate). At this point, sulphate concentrations remain constant, and nitrate increases with aerosol water content.

This sulphate-ammonium-nitrate-water equilibrium explains the behaviour of the inorganic species. For the highest RH case (H1RH), NO_3^- concentration shows a considerable increase while SO_4^{2-} slightly increases. This could be influenced by an increase of the RH favouring the NO_3^- formation together with a high sulphate concentration for which most of the sulphate

275   has been neutralized.

However, in the case with a reduction of the RH in a 10 % (L10RH), NO_3^- displays a similar concentration as the base case at surface levels and higher at levels above 800 hPa. Meanwhile, SO_4^{2-} concentrations are much higher than for the base case. Sulphate concentrations are favoured by its low deliquescence point which promotes its formation. In spite of that, at higher levels, sulphate concentrations were at the point in which most of the sulphate has been neutralized favouring NO_3^- formation,

280   producing higher NO_3^- concentrations in the L10RH case.

The H05RH (RH scaled to 1.005) experiment shows optical properties and concentration profiles closer to the base case, which can be caused by the low RH modification, so that inorganic species are not highly affected by this change.

Changes in the profiles of inorganic species do not clarify the results found for the modifications in the profiles of optical properties (and AOD). These modifications are led by changes in SOA. In both H1RH (RH scaled to 1.1) and L10RH (RH

285   scaled to 0.9), SOA profiles depict an increase in their concentrations resulting in an increase of α and hence AOD. Moreover, this increase is higher for the L10RH case. This positive variation in SOA profiles are explained by the use of the VBS mechanism (Ahmadov et al., 2012). As pointed out by Tuccella et al. (2015), in this mechanism volatile organic compounds(VOC) are oxidized by reactions with the hidroxy radical (OH), O_3, and nitrate radical (NO_3^-, producing organic mass in two different regimes of high and low NO_x). In the former, organic peroxy radicals react with nitrogen monoxide (NO); conversely, in the

290   latter organic peroxy radicals react with other organic peroxy radicals. The organic matter produced is partitioned into aerosol and gas phase assuming a pseudo-ideal partition.

     Thus, SOA profiles for the RH case depict two different types of behaviour: (1) Above 950 hPa (around the PBL height, see Figure 1 in the Supplementary Material,) the shape of the NO_x and SOA profiles are similar, and thus, at these vertical levels, variations in SOA concentrations may be due to the effect described by Sarrafzadeh et al. (2016): an increase in NO_x

295   concentrations at low-NO_x conditions (less than 30 ppb or around 55 $\mu g\ m^{-3}$); (2) Below 950 hPa the RH effect is added to the effect of NO_x described above in (1). Therefore, in the H1RH case, SOA are higher because the concentration of this species increases due to NO_x oxidation and RH, meanwhile in the L10RH case the positive variation of the concentration of SOA caused by the RH is limited.

     Over the MIN-AOD, the RH scaled to 0.9 (L10RH; NMAE > 0.6 except for SEA, 0.1) should be highlighted. Despite

300   L10RH does not provokes a strong difference in AOD, changes in organic species are relatively strong and are similar to those changes in β profile. A reduction of RH may favour the increase of the concentration of these species. α profile is similar to NO_3^-. In this case, these changes could be due to the actions of the nitrate-ammonia-sulphate equilibrium.

     Finally, to elucidate the response of the different experiments over a downwind location, profiles over Moscow are shown in Figure 7. The response for most of the experiments is similar as over the MAX-AOD location; but in this case L10RH (RH

305   scaled to 0.9) experiment shows a stronger response (NMAE > 1.5 for most of the variables) due to higher NO_3^- concentrations. Over this location RH is higher than over the MAX-AOD, favouring the formation of NO_3^-. POA displays higher concentrations for the L10RH case, likely due to a competition of SOA formation between NO_3^- and POA.

3.2.2   Sensitivity to dry deposition

Regarding dry deposition, the no dry deposition case (NO_DD) shows an increase in the AOD over the target area and displays

310   higher α and β values than for the base case at near-surface levels. However, above 950 hPa (around the PBL height, see Figure 1 in the Supplementary Material), the optical profiles decrease to levels lower than those for the base case. Despite this decrease aloft, total AOD increases (Figure 2) likely because the highest concentrations for chemical species are located at these levels. With respect to the different species, all of them present higher concentrations than the base case, in particular at levels below 950 hPa. MAE (NMAE) of α and β for this experiment are 0.0283 (1.1) and 0.0008 (1.1, Figure 4).

315   Changes in dry deposition experiments occur in those modes where modifications were implemented (Figure 4 in the Supplementary Material). When modifying the accumulation mode, the Aiken mode does not present important changes and thus the observed variations come from the accumulation mode. However, when modifications are implemented in the Aitken mode,

both modes are affected, since particles in the Aitken mode quickly experience coagulation processes and turn into particles in the accumulation mode.

320   A higher AOD is also found for the LDDV_AIT case (low dry deposition velocity in the Aitken mode). For this experiment, α (MAE 0.0205 and NMAE 0.8) and β (MAE 0.0005 and NMAE 0.7) exhibit higher values at the surface (around 1000 hPa) and between 900 and above 600 hPa. With respect to the profile of the different species, those emitted directly into the atmosphere (primary species) present higher concentrations than the base case at surface levels (around 1000 hPa and below 800 hPa, respectively). This is observed for POA (MAE 2.1988 and NMAE 0.7) and SEA (MAE 0.0154 and NMAE 0.4).

325   However, those species which are not directly emitted but are products of atmospheric chemistry (secondary aerosols), as SOA (NMAE > 0.8 and MAE 0.2283) and most of the secondary inorganic species have their concentrations peak higher than those in the base case between 900 and 600 hPa. These two facts explain the response of the profiles for the optical properties.

As expected, both high DDV experiments (HDDV_AIT and HDDV_ACC, in the Aitken and the accumulation mode respectively) exhibit a reduction of AOD, in particular over the fires area. The response of the optical properties profiles is similar

330   for both cases and for most of the species. For example, MAE (NMAE) are 0.0365 (0.8) and 0.0392 (1.5) for α. Only SEA shows a different behaviour between the increase of DDV for Aitken (NMAE 0.7) or accumulation mode (NMAE 0.8). The reduction of the total concentration of SEA is higher when DDV is modified in the accumulation mode. This is produced because this species presents most of its concentrations in the Greenfield gap, the accumulation and the coarse mode and not in Aitken. Regarding organic species (EC, POA and SOA), concentrations are a bit lower when the DDV is modified in

335   the accumulation mode, probably because most of the mass of these species is in this mode (NMAE around 1.4 for all of them). This response is similar to those experiments for SO_4^{2-}, but it is the contrary for NO_3^- because of the the action of the nitrate-sulphate-ammonium equilibrium.

The low dry deposition velocity in the accumulation mode (LDDV_ACC) experiment does not show the *a priori* expected response. AOD decreases over the fires; also optical properties profiles displays lower values: MAE (NMAE) 0.0331(1.3) for α

340   and 0.001(1.3) for β. When the profiles are analyzed, the response differs between species. EC, POA and NO_3^- shows a slight reduction in their concentration, and SOA exhibits a large reduction. Conversely, SO_4^{2-} and SEA display higher concentrations, in particular, at near-surface levels. The response of these latter is the expected when DDV is decreased in the accumulation mode but, despite this increase, the decrease of AOD is the result of the large reduction of SOA concentrations (NMAE 1.1). These SOA reductions may occur due to the increase in SO_4^{2-} concentrations (NMAE 1). By modifying the DDV, SO_4^{2-}

345   concentrations increase, then the nitrate-sulphate-ammonium equilibrium results in a reduction of NO_3^-, which influences SOA formation (as explained above) by decreasing their concentration.

Due to the different behaviour over the MIN-AOD location with respect to those areas affected by wildfires, the no dry deposition (NO_DD; NMAE > 0.9 for all the variables) should be highlighted. For NO_DD, β profile is similar to the profiles of organic species (EC, POA and SOA) while α is similar to NO_3^-. Organic species present a higher concentration when dry

350   deposition is turned off, resulting in an increase of β. However, NO_3^- decreases, probably due to its competition with SO_4^{2-} (which increases), leading to a decrease close to the surface of α. However, these changes in optical properties profiles are not highly represented by a strong modification of total AOD.

Atmospheric
Chemistry
and Physics
Discussions

Over the Moscow location, the NO_DD experiment also displays a strong response (NMAE > 1 for all the variables). This response is explained by an increase in the concentration of all the species, in particular, at the surface due to the effect of

355   turning off dry deposition resulting in an increase of α and β.

3.2.3   Sensitivity to sub-grid convective transport

When sub-grid convection is modified, in both experiments NO_CONV_TR (convective transport turned off) and HCONV_TR (scaled to 1.5) there is an AOD reduction over the fire area. This decrease is also reflected in optical properties and for most of the species (NMAE > 0.8 in both experiments) except SO_4^{2-}. For these species, the NO_CONV_TR experiment exhibits

360   a concentration profile similar to the base case with slightly higher concentrations at surface levels and lower at higher levels (NMAE 0.4). However, the SO_4^{2-} concentration profile for the HCONV_TR experiment shows lower concentrations (NMAE 1.2). Both responses could be caused by modifications in sub-grid convective transport. When this transport is turned off there is a decrease in the particle mixing in the atmosphere and small differences with the base case are found. However, when this transport is increased, involving an increase in all-direction convective transport and not only updraft convection, there is a

365   higher mixing of particles. This fact can favour the transport to levels closer to the surface and then enhance the deposition processes.

For the HCONV_TR experiment, the behaviour of SO_4^{2-} is similar to the rest of the species. Thus, the modification in sub-grid convective transport controls the response of this experiment. However, for the NO_CONV_TR test, the rest of the species behave differently as SO_4^{2-}. NO_3^- strongly decreases due to the effect of the nitrate-ammonium-sulphate equilibrium in

370   which the sulphate is an obstacle for NO_3^- formation. This low NO_3^- concentration results in a decrease of the SOA formation and consequently its concentration. This finally leads to a decrease of α and AOD. The response of LCONV_TR (convective transport scaled to 0.5) shows a transition between the two extreme cases (NMAE around 1 for all of the variables except SEA, 0.1, and SO_4^{2-}, 0.4).

Over the MIN-AOD location, the behaviour observed for the LCONV_TR experiment (convective transport scaled to 0.5)

375   is also noteworthy albeit NMAE does not have a strong response. AOD is not strongly modified but the profiles of optical properties show a peak in their profiles around the PBL height. This peak is due to an increase in the concentrations of EC, POA, SOA and NO_3^-. For the organic species this increase can be due to the modification in the sub-grid convective transport. The presence of these species at this level seems to favour the formation of NO_3^- instead of SO_4^{2-}.

3.2.4   Sensitivity to wet scavenging

380   The modification of wet scavenging over the MAX-AOD location displays a slight reduction of AOD, which is the result of lower α and reduced concentration of species above the PBL (at $950\,\mathrm{hPa}$). NMAE is < 0.8 for most of the studied variables. This reduction is observed despite the inorganic species (SEA, NO_3^-, NH_4^- and SO_4^{2-}) show higher concentrations at surface levels. SOA also displays a higher concentration below the PBL but with smaller changes than for inorganic species. This highlights the high impact of organic species on optical properties. All the observed changes can be attributed to changes in

385   the aqueous phase reactions because over these locations stratiform clouds were not present.

To conduct the analysis where clouds were formed during the 2010 wildfires episode, the MIN-AOD location is shown in Figure 5. Over this location, the NO_WS experiment is that with the strongest response regarding optical properties profiles and concentrations for different species. NMAE is above 1.5 for all the studied variables. The profiles of optical properties depict much higher values than for the base case, which are also observed in all of the species. This could be due to the fact

390   that over this area stratiform clouds were present, so the effect of wet scavenging is important over this location.

It should also be highlighted that over the MIN-AOD and Moscow spots, EC and POA profiles of the assessed experiments show larger differences between them than over the MAX-AOD. This fact could be explained because over these locations these species are not being directly emitted. Moreover, the farther the location is, the larger the differences are.

4   Summary and Conclusions

395   Aerosol optical properties (e.g. AOD) are highly influenced by the vertical distribution of atmospheric aerosols, which also condition the representation of ARI and ACI processes and their uncertainty. Thus, a key issue in climate modelling is the assessment of the uncertainty in the representation of aerosol optical properties. In order to reduce (or, at least, quantify) this uncertainty, this work assesses the sensitivity of aerosol optical properties and the aerosol vertical distribution to key physical processes. To achieve this objective, sensitivity runs modifying RH, dry deposition, sub-grid convective transport and wet

400   scavenging have been carried out during the 2010 Russian heatwave/wildfires episode with the WRF-Chem regional fully-coupled model.

Results indicate that there is a non-linear response of AOD to different key processes. For example, both an increase and a decrease in the RH results in higher AOD values. A similar non-linear response is found when reducing the dry deposition velocity; in particular, for the accumulation mode, where the concentration of several species increases (a decrease might be

405   *a priori* expected). Also the modifications in the sub-grid convective transport exhibit a non-linear response because both the increase and offset of this process leads to a reduction in the AOD over the fire area.

With respect to the quantification of the sensitivity, changes in RH of 0.9 lead to the highest AOD differences (0.6). This high sensitivity is followed in relevance by vertical convective transport (with AOD differences around -0.4) and dry deposition (AOD differences up to -0.35 and 0.3). Similar results were previously found, among others, by Lee et al. (2013); Kipling et al.

410   (2016) using both different models and experiments; and by Weigum et al. (2016) using the WRF-Chem model as in this work.

However, when RH increases (1.005 or 1.01 scaling factors), the response is weaker (AOD differences lower than 0.15) than when RH decreases. This is because the scaling to high RH values is smaller since an important supersaturation is not realistic in climate models. When the RH slightly increases the AOD changes are conditioned by the water uptake by particles and hence modifying the size of particles by hygroscopic growth (see H05RH experiment). In this case, no large changes

415   in concentrations are found. Nevertheless, for larger modifications (H1RH), changes in AOD are dominated by changes in nitrate and SOA. These changes in SOA are controlled by two mechanisms of particles formation. (1) The first mechanism, the nitrate-ammonia-sulphate equilibrium, explains the changes found for SO_4^{2-} and NO_3^-. Summarizing, the amount of sulphate domains this equilibrium in which ammonia can neutralize nitrate only when there is a high concentration of ammonia and/or

low concentrations of sulphate. By this way, if most of the SO_4^{2-} concentration has been neutralized, an increase in RH favours

420   NO_3^- formation. Moreover, in low RH conditions, NO_3^- formation is possible only under low SO_4^{2-} concentrations. (2) The second mechanism which controls SOA formation is the implemented VBS mechanism (Ahmadov et al., 2012; Tuccella et al., 2015). In our experiments, VOC are oxidized by reactions with nitrate radical in the regime of low NO_x and SOA increases as NO_3^- concentrations, as described by Sarrafzadeh et al. (2016).

Dry deposition presents a higher impact for the accumulation mode (NMAE higher than 1.4) than for the Aitken mode

425   (NMAE around 1.3) because a higher mass of fire particles are emitted into this mode. Over the MAX-AOD location switching off the dry deposition does not have a strong impact on AOD, but it does over the rest of the domain. Over this location, particles are directly emitted into the atmosphere while over other locations transport governs the concentrations. In general, when dry deposition is suppressed or reduced, AOD increases and conversely when it is increased, AOD decreases. However, the response over the MAX-AOD location of the decrease of dry deposition for the accumulation mode is noticeable because

430   a decrease in the dry deposition in this mode significantly increases SO_4^{2-} concentrations. Thus, the nitrate-ammonia-sulphate equilibrium reduces NO_3^- leading to a reduction of SOA and then AOD.

The suppression and the increase of the vertical convective transport also presents an impact on the aerosol vertical distribution. When the vertical convective transport is increased all the species show a similar response. This modification implies an increase of the transport not only upwards but also in all directions, increasing the mixing of particles which can favour

435   the transport from upper layers to the surface, hence enhancing deposition. However, when the sub-grid convective transport is suppressed the nitrate-ammonia-sulphate equilibrium and the SOA formation mechanisms play an important role. A reduction in the vertical convective transport, which can reduce the mixing of particles, results in significant changes of AOD but over regions away from the sources (main emission areas), in particular, over the MIN-AOD spot.

Wet scavenging does not significantly impact the vertical aerosol mass due to the type of episode selected as case study

440   (heatwave with clear skies). There is an impact over the MIN-AOD location because this is a cloudy area during the period of the episode.

Regarding the LR, simulated values of this variable are remarkably different from those observed in the scientific literature. In those areas where high LR are expected due to the presence of biomass burning particles, simulations estimate lower LR and viceversa. It should be also pointed out that most of the species show relatively larger differences when they are considered far

445   away from the emissions areas. Thus, as pointed out by Lee et al. (2013), the uncertainty in aerosol microphysical processes becomes increasingly important in remote regions (far from the source of emissions).

To summarize, the sulphate-nitrate-SOA formation is the process with the largest sensitivity and hence the process whose uncertainty can have a larger impact on AOD representation. Changes in this process could come from modifications in RH, dry deposition or vertical convective transport. By itself, dry deposition also presents a high sensitivity which influences AOD

450   representation.

Last, it should be noticed that the processes evaluated here are not the only processes that might condition the uncertainty in aerosol properties. The selection of these experiments has been based on their relevance according to the available literature and their experimental design has been constrained by the high computational cost of these on-line coupled chemistry-

meteorological simulations. In this sense, further studies addressing the reduction of the demonstrated uncertainties are needed.

455   Reducing uncertainties of AOD and aerosol representation implies the reduction of uncertainties in the representation of aerosol effects, both ARI (by AOD) and ACI (by improvement in microphysical properties) providing more reliable weather predictions and climatic simulations.

Data availability.   The data is available upon contacting the corresponding author (pedro.jimenezguerrero@um.es)

Author contributions.   LP-P wrote the manuscript, with contributions from PJ-G. LP-P and PS designed the experiments; LP-P conducted

460   the numerical simulations and compiled all the experiments, with the support of RL-P. LP-P did the analysis, with the support of PS, RL-P and PJ-G.

Competing interests.   The authors declare no conflict of interest.

Atmospheric
Chemistry
and Physics

Discussions

References

Ackermann, I. J., Hass, H., Memmesheimer, M., Ebel, A., Binkowski, F. S., and Shankar, U.: Modal aerosol dynamics model for Europe:

470   Development and first applications, Atmospheric Environment, 32, 2981 – 2999, doi: 10.1016/S1352-2310(98)00006-5, 1998.

Ahmadov, R., McKeen, S. A., Robinson, A. L., Bahreini, R., Middlebrook, A. M., de Gouw, J. A., Meagher, J., Hsie, E.-Y., Edgerton, E.,
        Shaw, S., and Trainer, M.: A volatility basis set model for summertime secondary organic aerosols over the eastern United States in 2006,
        Journal of Geophysical Research: Atmospheres, 117, D06 301, doi: 10.1029/2011JD016831, 2012.

Altaratz, O., Bar-Or, R. Z., Wollner, U., and Koren, I.: Relative humidity and its effect on aerosol optical depth in the vicinity of convective

475   clouds, Environmental Research Letters, 8, 034 025, doi: 10.1088/1748-9326/8/3/034025, 2013.

Balzarini, A., Pirovano, G., Honzak, L., Żabkar, R., Curci, G., Forkel, R., Hirtl, M., San José, R., Tuccella, P., and Grell, G.: WRF-Chem
        model sensitivity to chemical mechanisms choice in reconstructing aerosol optical properties, Atmospheric Environment, 115, 604 – 619,
        doi: 10.1016/j.atmosenv.2014.12.033, 2015.

Baró, R., Lorente-Plazas, R., Montávez, J. P., and Jiménez-Guerrero, P.: Biomass burning aerosol impact on surface winds during the 2010

480   Russian heat wave, Geophysical Research Letters, 44, 1088 – 1094, doi: 10.1002/2016GL071484, 2017.

Barriopedro, D., Fischer, E. M., Luterbacher, J., Trigo, R. M., and García-Herrera, R.: The Hot Summer of 2010: Redrawing the Temperature
        Record Map of Europe, Science, 332, 220 – 224, doi: 10.1126/science.1201224, 2011.

Binkowski, F. S. and Shankar, U.: The regional particulate matter model: 1. Model description and preliminary results, Journal of Geophysical
        Research: Atmospheres, 100, 26 191 – 26 209, doi: 10.1029/95JD02093, 1995.

485 Bondur, V.: Satellite monitoring of wildfires during the anomalous heat wave of 2010 in Russia, Izvestiya, Atmospheric and Oceanic Physics,
        47, 1039 – 1048, doi: 10.1134/S0001433811090040, 2011.

Boucher, O.: Atmospheric Aerosols: Properties and Climate Impacts, Springer Netherlands, xVII, 311 pages, doi: 10.1007/
        978-94-017-9649-1, 2015.

Boucher, O., Randall, D., Artaxo, P., Bretherton, C., Feingold, G., Forster, P., Kerminen, V.-M., Kondo, Y., Liao, H., Lohmann, U., Rasch,

490   P., Satheesh, S., Sherwood, S., Stevens, B., and Zhang, X.: Clouds and aerosols, in: Climate Change 2013: The Physical Science Basis.
        Contribution of Working Group I to the Fifth Assessment Report of the Intergovernmental Panel on Climate Change, edited by Stocker,
        T., Qin, D., Plattner, G.-K., Tignor, M., Allen, S., Boschung, J., Nauels, A., Xia, Y., Bex, V., , and Midgley, P., pp. 571 – 657, Cambridge
        University Press, Cambridge University Press, Cambridge, United Kingdom and New York, NY, USA., 2013.

Charlson, R. J., Schwartz, S. E., Hales, J. M., Cess, R. D., Coakley, J. A., Hansen, J. E., and Hofmann, D. J.: Climate Forcing by Anthro-

495   pogenic Aerosols, Science, 255, 423 – 430, doi: 10.1126/science.255.5043.423, 1992.

Chubarova, N., Nezval', Y., Sviridenkov, I., Smirnov, A., and Slutsker, I.: Smoke aerosol and its radiative effects during extreme fire event
        over Central Russia in summer 2010, Atmospheric Measurement Techniques, 5, 557 – 568, doi: 10.5194/amt-5-557-2012, 2012.

Curci, G., Alyuz, U., Baró, R., Bianconi, R., Bieser, J., Christensen, J. H., Colette, A., Farrow, A., Francis, X., Jiménez-Guerrero, P., Im, U.,
        Liu, P., Manders, A., Palacios-Peña, L., Prank, M., Pozzoli, L., Sokhi, R., Solazzo, E., Tuccella, P., Unal, A., Vivanco, M. G., Hogrefe,

500   C., and Galmarini, S.: Modelling black carbon absorption of solar radiation: combining external and internal mixing assumptions, Atmo-
        spheric Chemistry and Physics, 19, 181 – 204, doi: 10.5194/acp-19-181-2019, 2019.

Diapouli, E., Popovicheva, O., Kistler, M., Vratolis, S., Persiantseva, N., Timofeev, M., Kasper-Giebl, A., and Eleftheriadis, K.: Physico-
        chemical characterization of aged biomass burning aerosol after long-range transport to Greece from large scale wildfires in Russia and
        surrounding regions, Summer 2010, Atmospheric Environment, 96, 393 – 404, doi: 10.1016/j.atmosenv.2014.07.055, 2014.

Atmospheric
Chemistry
and Physics
Discussions

505 Doherty, R. M., Stevenson, D. S., Collins, W. J., and Sanderson, M. G.: Influence of convective transport on tropospheric ozone and its
        precursors in a chemistry-climate model, Atmospheric Chemistry and Physics, 5, 3205 – 3218, doi: 10.5194/acp-5-3205-2005, 2005.

Easter, R. C., Ghan, S. J., Zhang, Y., Saylor, R. D., Chapman, E. G., Laulainen, N. S., Abdul-Razzak, H., Leung, L. R., Bian, X., and Zaveri,
        R. A.: MIRAGE: Model description and evaluation of aerosols and trace gases, Journal of Geophysical Research: Atmospheres, 109,
        D20 210, doi: 10.1029/2004JD004571, 2004.

510 Fast, J. D., Gustafson Jr., W. I., Easter, R. C., Zaveri, R. A., Barnard, J. C., Chapman, E. G., Grell, G. A., and Peckham, S. E.: Evolution of
        ozone, particulates, and aerosol direct radiative forcing in the vicinity of Houston using a fully coupled meteorology-chemistry-aerosol
        model, Journal of Geophysical Research: Atmospheres, 111, D21 305, doi: 10.1029/2005JD006721, 2006.

Fernald, F. G., Herman, B. M., and Reagan, J. A.: Determination of Aerosol Height Distributions by Lidar, Journal of Applied Meteorology,
        11, 482 – 489, https://doi.org/10.1175/1520-0450(1972)011<0482:DOAHDB>2.0.CO;2, 1972.

515 Forkel, R., Balzarini, A., Baró, R., Bianconi, R., Curci, G., Jiménez-Guerrero, P., Hirtl, M., Honzak, L., Lorenz, C., Im, U., Pérez, J. L.,
        Pirovano, G., San José, R., Tuccella, P., Werhahn, J., and Žabkar, R.: Analysis of the WRF-Chem contributions to AQMEII phase2
        with respect to aerosol radiative feedbacks on meteorology and pollutant distributions, Atmospheric Environment, 115, 630 – 645, doi:
        10.1016/j.atmosenv.2014.10.056, 2015.

Forkel, R., Brunner, D., Baklanov, A., Balzarini, A., Hirtl, M., Honzak, L., Jiménez-Guerrero, P., Jorba, O., Pérez, J. L., San José, R.,
520   Schöder, W., Tsegas, G., Werhahn, J., Wolke, R., and Žabkar, R.: A Multi-model Case Study on Aerosol Feedbacks in Online Coupled
        Chemistry-Meteorology Models Within the COST Action ES1004 EuMetChem, in: Air Pollution Modeling and its Application XXIV.
        Springer Proceedings in Complexity, pp. 23 – 28, Springer, Cham, 2016.

Forster, P., Ramaswamy, V., Artaxo, P., Berntsen, T., Betts, R., Fahey, D., Haywood, J., Lean, J., Lowe, D., Myhre, G., Nganga, J., Prinn,
        R., Raga, G., Schulz, M., and Dorland, R. V.: Changes in Atmospheric Constituents and in Radiative Forcing, in: Climate Change 2013:
525   The Physical Science Basis. Contribution of Working Group I to the Fouth Assessment Report of the Intergovernmental Panel on Climate
        Change, edited by Solomon, S., Qin, D., Manning, M., Chen, Z., Marquis, M., Averyt, K., M.Tignor, and Miller, H., pp. 129 – 234,
        Cambridge University Press, Cambridge, United Kingdom and New York, NY, USA, 2007.

Galmarini, S., Hogrefe, C., Brunner, D., Makar, P., and Baklanov, A.: Preface, Atmospheric Environment, 115, 340 – 344, doi: 10.1016/j.
        atmosenv.2015.06.009, 2015.

530 Geiger, H., Barnes, I., Bejan, I., Benter, T., and Spittler, M.: The tropospheric degradation of isoprene: an updated module for the regional
        atmospheric chemistry mechanism, Atmospheric Environment, 37, 1503 – 1519, doi: https://doi.org/10.1016/S1352-2310(02)01047-6,
        2003.

Ginoux, P., Horowitz, L. W., Ramaswamy, V., Geogdzhayev, I. V., Holben, B. N., Stenchikov, G., and Tie, X.: Evaluation of aerosol distribu-
        tion and optical depth in the Geophysical Fluid Dynamics Laboratory coupled model CM2.1 for present climate, Journal of Geophysical
535   Research: Atmospheres, 111, D22 210, doi: 10.1029/2005JD006707, 2006.

Gorchakov, G., Sitnov, S., Sviridenkov, M., Semoutnikova, E., Emilenko, A., Isakov, A., Kopeikin, V., Karpov, A., Gorchakova, I., Verichev,
        K., Kurbatov, G., and Ponomareva, T.: Satellite and ground-based monitoring of smoke in the atmosphere during the summer wildfires in
        European Russia in 2010 and Siberia in 2012, International Journal of Remote Sensing, 35, 5698 – 5721, doi: 10.1080/01431161.2014.
        945008, 2014.

540 Grell, G. A.: Prognostic Evaluation of Assumptions Used by Cumulus Parameterizations, Monthly Weather Review, 121, 764 – 787, doi:
        10.1175/1520-0493(1993)121<0764:PEOAUB>2.0.CO;2, 1993.

Grell, G. A. and Dévényi, D.: A generalized approach to parameterizing convection combining ensemble and data assimilation techniques, Geophysical Research Letters, 29, doi: 10.1029/2002GL, 2002.

Grell, G. A. and Freitas, S. R.: A scale and aerosol aware stochastic convective parameterization for weather and air quality modeling,
545   Atmospheric Chemistry and Physics, 14, 5233 – 5250, doi: 10.5194/acp-14-5233-2014, 2014.

Grell, G. A., Dudhia, J., and Stauffer, D. R.: A description of the fifth-generation Penn State/NCAR mesoscale model (MM5), Tech. rep., Mesoscale and Microscale Meteorology Division, National Center for Atmospheric Research, pages 121, doi: 10.5065/D60Z716B, 1994.

Grell, G. A., Peckham, S. E., Schmitz, R., McKeen, S. A., Frost, G., Skamarock, W. C., and Eder, B.: Fully coupled "online" chemistry within the WRF model, Atmospheric Environment, 39, 6957 – 6975, doi: 10.1016/j.atmosenv.2005.04.027, 2005.

550   Hong, S.-Y., Noh, Y., and Dudhia, J.: A New Vertical Diffusion Package with an Explicit Treatment of Entrainment Processes, Monthly Weather Review, 134, 2318 – 2341, doi: 10.1175/MWR3199.1, 2006.

Iacono, M. J., Delamere, J. S., Mlawer, E. J., Shephard, M. W., Clough, S. A., and Collins, W. D.: Radiative forcing by long-lived greenhouse gases: Calculations with the AER radiative transfer models, Journal of Geophysical Research: Atmospheres, 113, D13 103, doi: 10.1029/2008JD009944, 2008.

555   Im, U., Bianconi, R., Solazzo, E., Kioutsioukis, I., Badia, A., Balzarini, A., Baró, R., Bellasio, R., Brunner, D., Chemel, C., Curci, G., Flemming, J., Forkel, R., Giordano, L., Jiménez-Guerrero, P., Hirtl, M., Hodzic, A., Honzak, L., Jorba, O., Knote, C., Kuenen, J. J., Makar, P. A., Manders-Groot, A., Neal, L., Pérez, J. L., Pirovano, G., Pouliot, G., Jose, R. S., Savage, N., Schroder, W., Sokhi, R. S., Syrakov, D., Torian, A., Tuccella, P., Werhahn, J., Wolke, R., Yahya, K., Žabkar, R., Zhang, Y., Zhang, J., Hogrefe, C., and Galmarini, S.: Evaluation of operational on-line-coupled regional air quality models over Europe and North America in the context of AQMEII phase 2.
560   Part I: Ozone, Atmospheric Environment, 115, 404 – 420, doi: 10.1016/j.atmosenv.2014.09.042, 2015a.

Im, U., Bianconi, R., Solazzo, E., Kioutsioukis, I., Badia, A., Balzarini, A., Baró, R., Bellasio, R., Brunner, D., Chemel, C., Curci, G., van der Gon, H. D., Flemming, J., Forkel, R., Giordano, L., Jiménez-Guerrero, P., Hirtl, M., Hodzic, A., Honzak, L., Jorba, O., Knote, C., Makar, P. A., Manders-Groot, A., Neal, L., Pérez, J. L., Pirovano, G., Pouliot, G., Jose, R. S., Savage, N., Schroder, W., Sokhi, R. S., Syrakov, D., Torian, A., Tuccella, P., Wang, K., Werhahn, J., Wolke, R., Žabkar, R., Zhang, Y., Zhang, J., Hogrefe, C., and Galmarini, S.: Evaluation
565   of operational online-coupled regional air quality models over Europe and North America in the context of AQMEII phase 2. Part II: Particulate matter, Atmospheric Environment, 115, 421 – 441, doi: 10.1016/j.atmosenv.2014.08.072, 2015b.

Inness, A., Baier, F., Benedetti, A., Bouarar, I., Chabrillat, S., Clark, H., Clerbaux, C., Coheur, P., Engelen, R. J., Errera, Q., Flemming, J., George, M., Granier, C., Hadji-Lazaro, J., Huijnen, V., Hurtmans, D., Jones, L., Kaiser, J. W., Kapsomenakis, J., Lefever, K., Leitão, J., Razinger, M., Richter, A., Schultz, M. G., Simmons, A. J., Suttie, M., Stein, O., Thépaut, J.-N., Thouret, V., Vrekoussis, M., Zerefos, C.,
570   and the MACC team: The MACC reanalysis: an 8 yr data set of atmospheric composition, Atmospheric Chemistry and Physics, 13, 4073 – 4109, doi: 10.5194/acp-13-4073-2013, 2013.

Kipling, Z., Stier, P., Johnson, C. E., Mann, G. W., Bellouin, N., Bauer, S. E., Bergman, T., Chin, M., Diehl, T., Ghan, S. J., Iversen, T., Kirkevåg, A., Kokkola, H., Liu, X., Luo, G., van Noije, T., Pringle, K. J., vonÂ Salzen, K., Schulz, M., Seland, Ø., Skeie, R. B., Takemura, T., Tsigaridis, K., and Zhang, K.: What controls the vertical distribution of aerosol? Relationships between process sensitivity
575   in HadGEM3–UKCA and inter-model variation from AeroCom Phase II, Atmospheric Chemistry and Physics, 16, 2221 – 2241, doi: 10.5194/acp-16-2221-2016, 2016.

Kong, X., Forkel, R., Sokhi, R. S., Suppan, P., Baklanov, A., Gauss, M., Brunner, D., Baró, R., Balzarini, A., Chemel, C., Curci, G., Jiménez-Guerrero, P., Hirtl, M., Honzak, L., Im, U., Pérez, J. L., Pirovano, G., San José, R., Schlünzen, K. H., Tsegas, G., Tuccella, P., Werhahn, J.,

Žabkar, R., and Galmarini, S.: Analysis of meteorology-chemistry interactions during air pollution episodes using online coupled models
within AQMEII phase-2, Atmospheric Environment, 115, 527 – 540, doi: 10.1016/j.atmosenv.2014.09.020, 2015.

Konovalov, I. B., Beekmann, M., Kuznetsova, I. N., Yurova, A., and Zvyagintsev, A. M.: Atmospheric impacts of the 2010 Russian wildfires:
integrating modelling and measurements of an extreme air pollution episode in the Moscow region, Atmospheric Chemistry and Physics,
11, 10 031 – 10 056, doi: 10.5194/acp-11-10031-2011, 2011.

Kramm, G., Beheng, K. D., and Müller, H.: Vertical transport of polydispersed aerosol particles in the atmospheric surface layer, in: Precipita-
tion Scavenging and Atmosphere-Surface Exchange Processes, edited by Schwartz, S. and Slinn, W., vol. 2, pp. 1125 – 1141, Hemisphere
New York, 1992.

Kuenen, J. J. P., Visschedijk, A. J. H., Jozwicka, M., and Denier van der Gon, H. A. C.: TNO-MACC_II emission inventory; a multi-year
(2003–2009) consistent high-resolution European emission inventory for air quality modelling, Atmospheric Chemistry and Physics, 14,
10 963 – 10 976, doi: 10.5194/acp-14-10963-2014, 2014.

Lau, W. K. M. and Kim, K.-M.: The 2010 Pakistan Flood and Russian Heat Wave: Teleconnection of Hydrometeorological Extremes, Journal
of Hydrometeorology, 13, 392 – 403, doi: 10.1175/JHM-D-11-016.1, 2012.

Lee, L. A., Pringle, K. J., Reddington, C. L., Mann, G. W., Stier, P., Spracklen, D. V., Pierce, J. R., and Carslaw, K. S.: The magnitude and
causes of uncertainty in global model simulations of cloud condensation nuclei, Atmospheric Chemistry and Physics, 13, 8879 – 8914,
doi: 10.5194/acp-13-8879-2013, 2013.

Makar, P., Gong, W., Hogrefe, C., Zhang, Y., Curci, G., Žabkar, R., Milbrandt, J., Im, U., Balzarini, A., Baró, R., Bianconi, R., Cheung,
P., Forkel, R., Gravel, S., Hirtl, M., Honzak, L., Hou, A., Jiménez-Guerrero, P., Langer, M., Moran, M., Pabla, B., Pérez, J., Pirovano,
G., José, R. S., Tuccella, P., Werhahn, J., Zhang, J., and Galmarini, S.: Feedbacks between air pollution and weather, part 2: Effects on
chemistry, Atmospheric Environment, 115, 499 – 526, doi: 10.1016/j.atmosenv.2014.10.021, 2015a.

Makar, P., Gong, W., Milbrandt, J., Hogrefe, C., Zhang, Y., Curci, G., Žabkar, R., Im, U., Balzarini, A., Baró, R., Bianconi, R., Cheung,
P., Forkel, R., Gravel, S., Hirtl, M., Honzak, L., Hou, A., Jiménez-Guerrero, P., Langer, M., Moran, M., Pabla, B., Pérez, J., Pirovano,
G., San José, R., Tuccella, P., Werhahn, J., Zhang, J., and Galmarini, S.: Feedbacks between air pollution and weather, Part 1: Effects on
weather, Atmospheric Environment, 115, 442 – 469, doi: 10.1016/j.atmosenv.2014.12.003, 2015b.

Mielonen, T., Aaltonen, V., Lihavainen, H., Hyvärinen, A.-P., Arola, A., Komppula, M., and Kivi, R.: Biomass Burning Aerosols Observed
in Northern Finland during the 2010 Wildfires in Russia, Atmosphere, 4, 17 – 34, doi: 10.3390/atmos4010017, 2013.

Morrison, H., Thompson, G., and Tatarskii, V.: Impact of Cloud Microphysics on the Development of Trailing Stratiform Precipitation in
a Simulated Squall Line: Comparison of One- and Two-Moment Schemes, Monthly Weather Review, 137, 991 – 1007, doi: 10.1175/
2008MWR2556.1, 2009.

Müller, D., Ansmann, A., Mattis, I., Tesche, M., Wandinger, U., Althausen, D., and Pisani, G.: Aerosol-type-dependent lidar ratios observed
with Raman lidar, Journal of Geophysical Research: Atmospheres, 112, https://doi.org/10.1029/2006JD008292, 2007.

Palacios-Peña, L., Baró, R., Guerrero-Rascado, J. L., Alados-Arboledas, L., Brunner, D., and Jiménez-Guerrero, P.: Evaluating the represen-
tation of aerosol optical properties using an online coupled model over the Iberian Peninsula, Atmospheric Chemistry and Physics, 17,
277 – 296, doi: 10.5194/acp-17-277-2017, 2017.

Palacios-Peña, L., Baró, R., Baklanov, A., Balzarini, A., Brunner, D., Forkel, R., Hirtl, M., Honzak, L., López-Romero, J. M., Montávez,
J. P., Pérez, J. L., Pirovano, G., San José, R., Schröder, W., Werhahn, J., Wolke, R., Žabkar, R., and Jiménez-Guerrero, P.: An assessment
of aerosol optical properties from remote-sensing observations and regional chemistry–climate coupled models over Europe, Atmospheric
Chemistry and Physics, 18, 5021 – 5043, doi: 10.5194/acp-18-5021-2018, 2018.

Atmospheric
Chemistry
and Physics
Discussions
Open Access
EGU

Palacios-Peña, L., Jiménez-Guerrero, P., Baró, R., Balzarini, A., Bianconi, R., Curci, G., Landi, T. C., Pirovano, G., Prank, M., Riccio, A., Tuccella, P., and Galmarini, S.: Aerosol optical properties over Europe: an evaluation of the AQMEII Phase 3 simulations against satellite observations, Atmospheric Chemistry and Physics, 19, 2965 – 2990, doi: 10.5194/acp-19-2965-2019, 2019.

620 Penner, J. E., Andreae, M. O., Annegarn, H., Barrie, L., Feichter, J., Hegg, D., Jayaraman, A., Leaitch, R., Murphy, D., Nganga, J., Pitari, G., et al.: Aerosols, their direct and indirect effects, in: Climate Change 2001: The Scientific Basis. Contribution of Working Group I to the Third Assessment Report of the Intergovernmental Panel on Climate Change, edited by Houghton, J. T., Ding, Y., Griggs, D. J., Noguer, M., Linden, P. J. v. d., and Xiaosu, D., pp. 289 – 348, Cambridge University Press, Cambridge University Press, Cambridge, United Kingdom and New York, NY, USA., 2001.

625 Péré, J. C., Bessagnet, B., Mallet, M., Waquet, F., Chiapello, I., Minvielle, F., Pont, V., and Menut, L.: Direct radiative effect of the Russian wildfires and its impact on air temperature and atmospheric dynamics during August 2010, Atmospheric Chemistry and Physics, 14, 1999 – 2013, doi: 10.5194/acp-14-1999-2014, 2014.

Péré, J. C., Bessagnet, B., Pont, V., Mallet, M., and Minvielle, F.: Influence of the aerosol solar extinction on photochemistry during the 2010 Russian wildfires episode, Atmospheric Chemistry and Physics, 15, 10 983 – 10 998, doi: 10.5194/acp-15-10983-2015, 2015.

630 Pleim, J., Venkatram, A., and Yamartino, R.: ADOM/TADAP Model Development Program: The Dry Deposition Module, Atmospheric Environment (1967), 14, 1013 – 1016, 1984.

Portin, H., Mielonen, T., Leskinen, A., Arola, A., Pärjälä, E., Romakkaniemi, S., Laaksonen, A., Lehtinen, K., and Komppula, M.: Biomass burning aerosols observed in Eastern Finland during the Russian wildfires in summer 2010 – Part 1: In-situ aerosol characterization, Atmospheric Environment, 47, 269 – 278, doi: 10.1016/j.atmosenv.2011.10.067, 2012.

635 Pouliot, G., Pierce, T., van der Gon, H. D., Schaap, M., Moran, M., and Nopmongcol, U.: Comparing emission inventories and model-ready emission datasets between Europe and North America for the AQMEII project, Atmospheric Environment, 53, 4 – 14, doi: 10.1016/j. atmosenv.2011.12.041, 2012.

Pouliot, G., van der Gon, H. A. C. D., Kuenen, J., Zhang, J., Moran, M. D., and Makar, P. A.: Analysis of the emission inventories and model-ready emission datasets of Europe and North America for phase 2 of the AQMEII project, Atmospheric Environment, 115, 345 –
640 360, doi: 10.1016/j.atmosenv.2014.10.061, 2015.

Quan, J., Di, Z., Duan, Q., Gong, W., Wang, C., Gan, Y., Ye, A., and Miao, C.: An evaluation of parametric sensitivities of different meteorological variables simulated by the WRF model, Quarterly Journal of the Royal Meteorological Society, 142, 2925–2934, doi: 10.1002/qj.2885, 2016.

Rahmstorf, S. and Coumou, D.: Increase of extreme events in a warming world, Proceedings of the National Academy of Sciences, 108,
645 17 905 – 17 909, doi: 10.1073/pnas.1101766108, 2011.

Randall, D. A., Wood, R. A., Bony, S., Colman, R., Fichefet, T., Fyfe, J., Kattsov, V., Pitman, A., Shukla, J., Srinivasan, J., Stouffer, R. J., Sumi, A., and Taylor, K. E.: Climate models and their evaluation, in: Climate Change 2013: The Physical Science Basis. Contribution of Working Group I to the Fouth Assessment Report of the Intergovernmental Panel on Climate Change, edited by Solomon, S., Qin, D., Manning, M., Chen, A., Marquis, M., Averyt, K., Tignor, M., and Miller, H., pp. 589 – 662, Cambridge University Press, Cambridge
650 University Press, Cambridge, United Kingdom and New York, NY, USA., 2007.

Romakkaniemi, S., Arola, A., Kokkola, H., Birmili, W., Tuch, T., Kerminen, V.-M., Räisänen, P., Smith, J. N., Korhonen, H., and Laaksonen, A.: Effect of aerosol size distribution changes on AOD, CCN and cloud droplet concentration: Case studies from Erfurt and Melpitz, Germany, Journal of Geophysical Research: Atmospheres, 117, D07 202, doi: 10.1029/2011JD017091, 2012.

Atmospheric
Chemistry
and Physics
Discussions
Open Access
EGU

Safronov, A. N., Fokeeva, E. V., Rakitin, V. S., Grechko, E. I., and Shumsky, R. A.: Severe Wildfires Near Moscow, Russia in 2010: Modeling
655   of Carbon Monoxide Pollution and Comparisons with Observations, Remote Sensing, 7, 395 – 429, doi: 10.3390/rs70100395, 2015.

Sarrafzadeh, M., Wildt, J., Pullinen, I., Springer, M., Kleist, E., Tillmann, R., Schmitt, S. H., Wu, C., Mentel, T. F., Zhao, D., Hastie, D. R.,
and Kiendler-Scharr, A.: Impact of NO_x and OH on secondary organic aerosol formation from β-pinene photooxidation, Atmospheric
Chemistry and Physics, 16, 11 237 – 11 248, doi: 10.5194/acp-16-11237-2016, 2016.

Saxena, P., Hudischewskyj, A. B., Seigneur, C., and Seinfeld, J. H.: A comparative study of equilibrium approaches to the chemical charac-
660   terization of secondary aerosols, Atmospheric Environment (1967), 20, 1471 – 1483, doi: 10.1016/0004-6981(86)90019-3, 1986.

Schaap, M., Roemer, M., Sauter, F., Boersen, G., Timmermans, R., Builtjes, P. J. H., and Vermeulen, A. T.: LOTOS-EUROS: Documentation,
Tech. rep., TNO, 57 pages, 2005.

Schimel, D., Alves, D., Enting, I., Heimann, M., Joos, F., Raynaud, D., Wigley, T., Prather, M., Derwent, R., Ehhalt, D., Fraser, P., Sanhuenza,
E., Zhou, X., Jonas, P., Charlson, R., Rodhe, H., Sadasivan, S., Shine, K. P., Fouquart, Y., Ramaswamy, V., Solomon, S., Srinivasan, J.,
665   Albritton, D., Isaksen, I., Lal, M., and Wuebbles, D.: Radiative forcing of climate change, in: Climate Change 1996, Contribution of Work-
ing Group I to the Second Assessment Report of the Intergovernmental Panel on Climate Change, edited by Houghton, J. T., Meira Filho,
L. G., Callander, B. A., Harris, N., Kattenberg, A., and Maskell, K., Cambridge University Press, Cambridge, United Kingdom and New
York, NY, USA, 1996.

Sedlàček, J., Martius, O., and Knutti, R.: Influence of subtropical and polar sea-surface temperature anomalies on temperatures in Eurasia,
670   Geophysical Research Letters, 38, L12 803, doi: 10.1029/2011GL047764, 2011.

Seinfeld, J. H. and Pandis, S. N.: Atmospheric Chemistry and Physics: From Air Pollution to Climate Change, John Wiley & Sons, INC.,
Second edn., 1225 pages, 2006.

Slinn, S. and Slinn, W.: Predictions for particle deposition on natural waters, Atmospheric Environment (1967), 14, 1013 – 1016, doi:
10.1016/0004-6981(80)90032-3, 1980.

675   Soares, J., Sofiev, M., and Hakkarainen, J.: Uncertainties of wild-land fires emission in AQMEII phase 2 case study, Atmospheric Environ-
ment, 115, 361 – 370, doi: 10.1016/j.atmosenv.2015.01.068, 2015.

Sofiev, M., Vankevich, R., Lotjonen, M., Prank, M., Petukhov, V., Ermakova, T., Koskinen, J., and Kukkonen, J.: An operational system
for the assimilation of the satellite information on wild-land fires for the needs of air quality modelling and forecasting, Atmospheric
Chemistry and Physics, 9, 6833 – 6847, doi: 10.5194/acp-9-6833-2009, 2009.

680   Stier, P., Feichter, J., Kinne, S., Kloster, S., Vignati, E., Wilson, J., Ganzeveld, L., Tegen, I., Werner, M., Balkanski, Y., Schulz, M., Boucher,
O., Minikin, A., and Petzold, A.: The aerosol-climate model ECHAM5-HAM, Atmospheric Chemistry and Physics, 5, 1125 – 1156, doi:
10.5194/acp-5-1125-2005, 2005.

Stockwell, W. R., Kirchner, F., Kuhn, M., and Seefeld, S.: A new mechanism for regional atmospheric chemistry modeling, Journal of
Geophysical Research: Atmospheres, 102, 25 847 – 25 879, doi: 10.1029/97JD00849, 1997.

685   Tewari, M., Chen, F., Wang, W., Dudhia, J., LeMone, M., Mitchell, K., Ek, M., Gayno, G., Wegiel, J., and Cuenca, R.: Implementation and
verification of the unified NOAH land surface model in the WRF model, in: 20th conference on weather analysis and forecasting/16th
conference on numerical weather prediction, pp. 11 – 15, 2004.

Toll, V., Reis, K., Ots, R., Kaasik, M., Männik, A., Prank, M., and Sofiev, M.: SILAM and MACC reanalysis aerosol data used for simulating
the aerosol direct radiative effect with the NWP model HARMONIE for summer 2010 wildfire case in Russia, Atmospheric Environment,
690   121, 75 – 85, doi: 10.1016/j.atmosenv.2015.06.007, 2015.

Trenberth, K. E. and Fasullo, J. T.: Climate extremes and climate change: The Russian heat wave and other climate extremes of 2010, Journal of Geophysical Research: Atmospheres, 117, D17 103, doi: 10.1029/2012JD018020, 2012.

Tuccella, P., Curci, G., Visconti, G., Bessagnet, B., Menut, L., and Park, R. J.: Modeling of gas and aerosol with WRF/Chem over Europe: Evaluation and sensitivity study, Journal of Geophysical Research: Atmospheres, 117, D03 303, doi: 10.1029/2011JD016302, 2012.

Tuccella, P., Curci, G., Grell, G. A., Visconti, G., Crumeyrolle, S., Schwarzenboeck, A., and Mensah, A. A.: A new chemistry option in WRF-Chem v. 3.4 for the simulation of direct and indirect aerosol effects using VBS: evaluation against IMPACT-EUCAARI data, Geoscientific Model Development, 8, 2749 – 2776, doi: 10.5194/gmd-8-2749-2015, 2015.

van Donkelaar, A., Martin, R. V., Levy, R. C., da Silva, A. M., Krzyzanowski, M., Chubarova, N. E., Semutnikova, E., and Cohen, A. J.: Satellite-based estimates of ground-level fine particulate matter during extreme events: A case study of the Moscow fires in 2010, Atmospheric Environment, 45, 6225 – 6232, doi: https://doi.org/10.1016/j.atmosenv.2011.07.068, 2011.

Žabkar, R., Honzak, L., Skok, G., Forkel, R., Rakovec, J., Ceglar, A., and Žagar, N.: Evaluation of the high resolution WRF-Chem (v3.4.1) air quality forecast and its comparison with statistical ozone predictions, Geoscientific Model Development, 8, 2119 – 2137, doi: 10.5194/gmd-8-2119-2015, 2015.

Weigum, N., Schutgens, N., and Stier, P.: Effect of aerosol subgrid variability on aerosol optical depth and cloud condensation nuclei: implications for global aerosol modelling, Atmospheric Chemistry and Physics, 16, 13 619 – 13 639, doi: 10.5194/acp-16-13619-2016, 2016.

Wesely, M. L.: Parameterization of surface resistances to gaseous dry deposition in regional-scale numerical models, Atmospheric Environment (1967), 23, 1293 – 1304, doi: 10.1016/0004-6981(89)90153-4, 1989.

Witte, J. C., Douglass, A. R., da Silva, A., Torres, O., Levy, R., and Duncan, B. N.: NASA A-Train and Terra observations of the 2010 Russian wildfires, Atmospheric Chemistry and Physics, 11, 9287 – 9301, doi: 10.5194/acp-11-9287-2011, 2011.

Wong, D. C., Pleim, J., Mathur, R., Binkowski, F., Otte, T., Gilliam, R., Pouliot, G., Xiu, A., Young, J. O., and Kang, D.: WRF-CMAQ two-way coupled system with aerosol feedback: software development and preliminary results, Geoscientific Model Development, 5, 299 – 312, doi: 10.5194/gmd-5-299-2012, 2012.

Wooster, M. J., Roberts, G., Perry, G. L. W., and Kaufman, Y. J.: Retrieval of biomass combustion rates and totals from fire radiative power observations: FRP derivation and calibration relationships between biomass consumption and fire radiative energy release, Journal of Geophysical Research: Atmospheres, 110, D24 311, doi: 10.1029/2005JD006318, 2005.

Yoon, S.-C. and Kim, J.: Influences of relative humidity on aerosol optical properties and aerosol radiative forcing during ACE-Asia, Atmospheric Environment, 40, 4328 – 4338, doi: 10.1016/j.atmosenv.2006.03.036, 2006.

Zhang, K., O'Donnell, D., Kazil, J., Stier, P., Kinne, S., Lohmann, U., Ferrachat, S., Croft, B., Quaas, J., Wan, H., Rast, S., and Feichter, J.: The global aerosol-climate model ECHAM-HAM, version 2: sensitivity to improvements in process representations, Atmospheric Chemistry and Physics, 12, 8911 – 8949, doi: 10.5194/acp-12-8911-2012, 2012.

Zvyagintsev, A. M., Blum, O. B., Glazkova, A. A., Kotel'nikov, S. N., Kuznetsova, I. N., Lapchenko, V. A., Lezina, E. A., Miller, E. A., Milyaev, V. A., Popikov, A. P., Semutnikova, E. G., TarasovaI, O. A., and Shalygina, Y.: Anomalies of trace gases in the air of the European part of Russia and Ukraine in summer 2010, Atmospheric and Oceanic Optics, 24, 536 – 542, doi: 10.1134/S1024856011060145, 2011.

Atmospheric
Chemistry
and Physics

Open Access

EGU

Discussions

Table 1. WRF-Chem physical and chemical configuration used in the sensitivity tests.

Scheme	Option	Reference
Physic		
Microphysics	Morrison	Morrison et al. (2009)
SW & LW radiation	RRTM	Iacono et al. (2008)
Planetary boundary layer	YSU	Hong et al. (2006)
Cumulus	Grell-Freitas	Grell and Freitas (2014)
Soil	Noah	Tewari et al. (2004)
Chemistry		
Gas-phase	RACM-KPP	Stockwell et al. (1997) Geiger et al. (2003)
Aerosol	MADE/VBS	Ackermann et al. (1998) Tuccella et al. (2015)
Photolysis	Fast-J	Fast et al. (2006)
Dry Deposition		Wesely (1989)
Wet Deposition	grid-scale	
ARI & ACI	ON	

Table 2. Description of the experiments carried out to perform the sensitivity tests of aerosol to different processes; changes of relative humidity (RH), dry deposition (DDV), convective transport and wet scavenging.

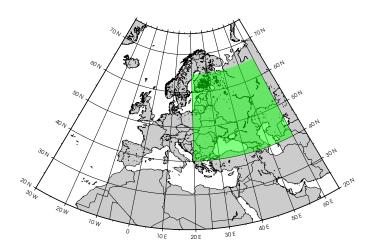| Experiment	Description
Base Case	–
L10RH	RH scaled to 0.9 in the aerosol module
H05RH	RH scaled to 1.005 in the aerosol module
H1RH	RH scaled to 1.01 in the aerosol module
NO_DD	No aerosol dry deposition (DD)
LDDV_AIT	DDV scaled to 0.5 for Aitken Mode
HDDV_AIT	DDV scaled to 2 for Aitken Mode
LDDV_ACC	DDV scaled to 0.1 for the Accumulation Mode
HDDV_ACC	DDV scaled to 10 for the Accumulation Mode
NO_CONV_TR	No sub-grid convective transport
LCONV_TR	Sub-grid convective transport scaled to 0.5
HCONV_TR	Sub-grid convective transport scaled to 1.5
NO_WS	No stratiform wet scavenging

Figure 1. Simulated domain (grey) and fire-affected target area (green box).
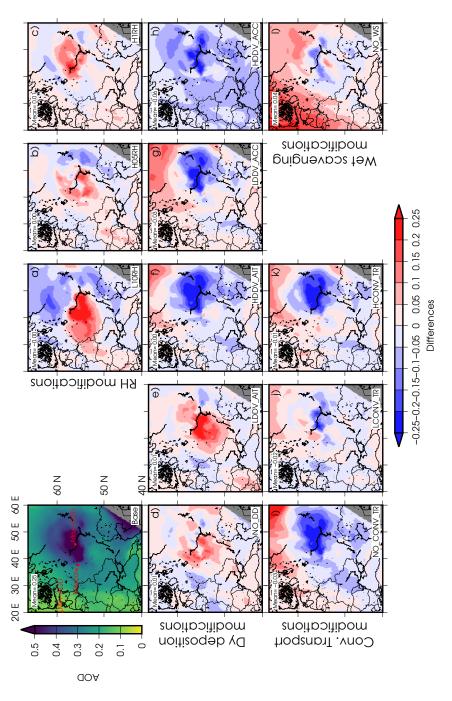
Figure 2. Modelled AOD at 550 nm for the base case (top-left) and mean relative differences between experiments and the base case. RH modifications at the top-right: a) scaled to 0.9 (L10RH); b) scaled to 1.005 (H05RH); and c) scaled to 1.01 (H1RH). Dry deposition modifications at the second row: d) the suppression (NO_DD); e) the low DDV for the Aitken mode (LDDV_AIT); f) the high (HDDV_AIT); g) the low DDV for the Accumulation mode (LDDV_ACC); and h) the high (HDDV_ACC). Sub-grid convective transport are in bottom-right row: i) the suppression (NO_CONV_TRANS); j) scaled to 0.5 (LCONV_TRANS) and k) scaled to 1.5 (HCONV_TRANS). Bottom-left panel, l), is the suppression of the wet scavenging.

Figure 3. Profiles over the Max-AOD location. Top row shows the α (left), β (centre) & LR (right). From second to bottom rows, columns display concentration of EC, POA, SOA, SEA, NO_3^-, NH_4^- & SO_4^{2-}. The second row is for total concentration; the third for dry; and the bottom for wet. The solid black line represents the base case. The blue color is for RH sensitivity: the dotted dark is the high in 1 % (H1RH); the dotted light, the high in 0.5 % (H05RH); and the dotted-dashed light, the low in 10 % (L10RH). The violet color is for dry deposition. The solid dark is the no dry deposition (NO_DD). The rest dark are for the modification of DDV in the Aitken mode: the dotted is the high (HDDV_AIT); and the dotted-dashed, the low (LDDV_AIT). Similar but in light violet is for the accumulation mode: the dotted is the high (HDDV_ACC); and the dotted-dashed, the low (DDV_ACC). The brown color is for sub-grid convective transport: the solid, without it (NO_CONV_TR); the dotted, the high case (HCONC_TR); and the dotted-dashed, the low (LCONV_TR). The solid green represents the wet scavenging turned off (NO_WS).
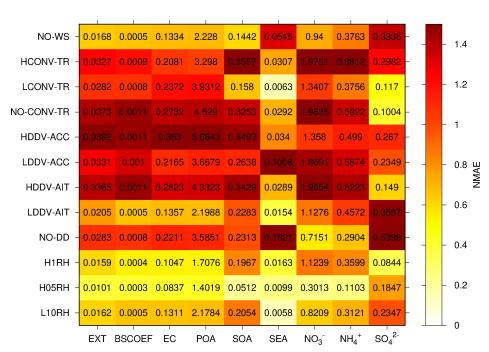
Figure 4. Normalized absolute differences (color) and absolute differences (numbers) between each experiment and the base case over the MAX-AOD location. Columns represent each variable and rows each experiment.
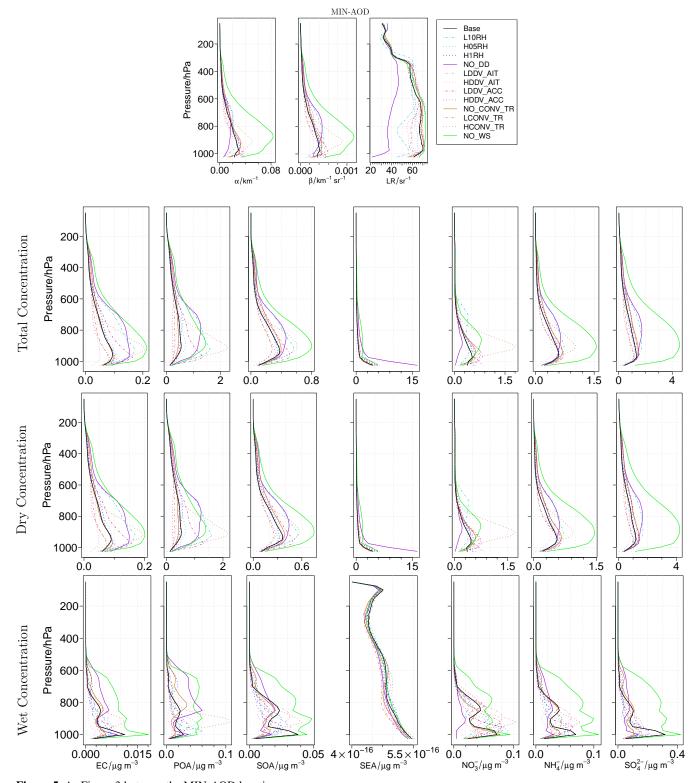
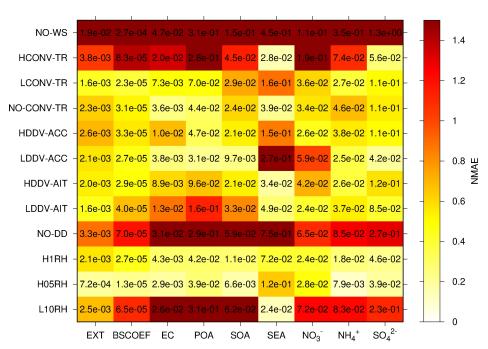**Figure 5.** As Figure 3 but over the MIN-AOD location.
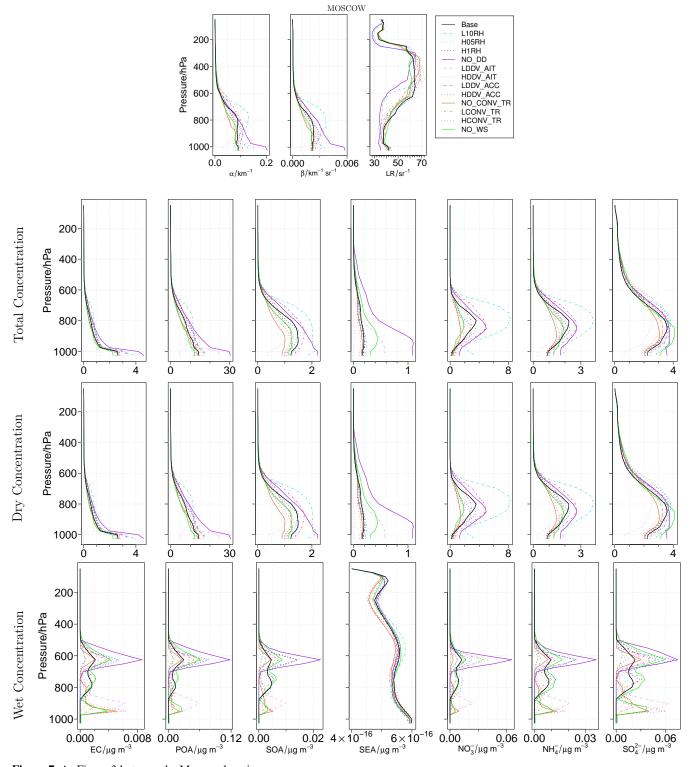
Figure 6. As Figure 4 but over MIN-AOD location.

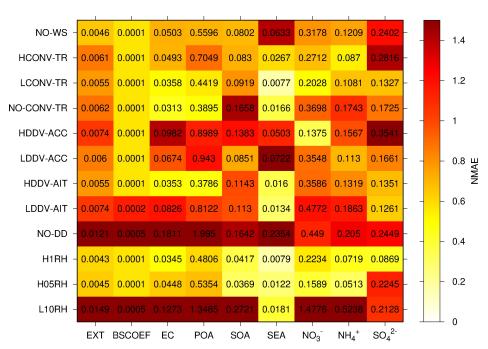**Figure 7.** As Figure 3 but over the Moscow location.

Atmospheric
Chemistry
and Physics
Discussions

Figure 8. As Figure 4 but over Moscow location.